BWCache: Accelerating Video Diffusion Transformers through Block-Wise Caching

Hanshuai Cui[1,2], **Zhiqing Tang**[*2], **Zhifei Xu** [1,2], **Zhi Yao** [2], **Wenyi Zeng** [1], **and Weijia Jia** [2]
[1]School of Artificial Intelligence, Beijing Normal University, Beijing 100875, China
[2]Institute of Artificial Intelligence and Future Networks, Beijing Normal University, Zhuhai 519087, China

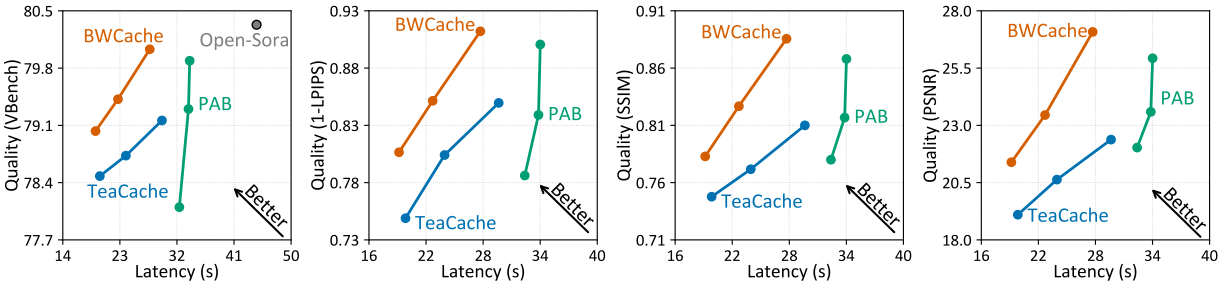

Figure 1: Quality-latency comparisons for video diffusion models. Visual quality versus latency curves are presented for the proposed BWCache method, PAB, and TeaCache using Open-Sora. BWCache demonstrates significantly superior visual quality and efficiency compared to both PAB and TeaCache. Latency is evaluated on a single NVIDIA A800 GPU for generating 51 frames, 480P videos.

Abstract

Recent advancements in Diffusion Transformers (DiTs) have established them as the state-of-the-art method for video generation. However, their inherently sequential denoising process results in inevitable latency, limiting real-world applicability. Existing acceleration methods either compromise visual quality due to architectural modifications or fail to reuse intermediate features at proper granularity. Our analysis reveals that DiT blocks are the primary contributors to inference latency. Across diffusion timesteps, the feature variations of DiT blocks exhibit a U-shaped pattern with high similarity during intermediate timesteps, which suggests substantial computational redundancy. In this paper, we propose Block-Wise Caching (BWCache), a training-free method to accelerate DiT-based video generation. BWCache dynamically caches and reuses features from DiT blocks across diffusion timesteps. Furthermore, we introduce a similarity indicator that triggers feature reuse only when the differences between block features at adjacent timesteps fall below a threshold, thereby minimizing redundant computations while maintaining visual fidelity. Extensive experiments on several video diffusion models demonstrate that BWCache achieves up to 2.24× speedup with comparable visual quality.

1 Introduction

Diffusion Models (DMs) Song and Ermon [2019], Ho et al. [2020], Dhariwal and Nichol [2021] have emerged as the predominant technology in Generative AI (GenAI) due to their ability to generate high-fidelity images and videos Rombach et al. [2022]. Early DMs primarily adopted the U-Net architecture Ronneberger et al. [2015], Ramesh et al. [2022], Saharia et al. [2022], Blattmann et al. [2023]. Recently, the success of Sora Brooks et al. [2024] has spurred the adoption of the Diffusion Transformer (DiT) architecture Peebles and Xie [2023], Bao et al. [2023] for video generation, achieving state-of-the-art performance. Video generation with DiT requires the sequential computation of multiple DiT

*Corresponding author

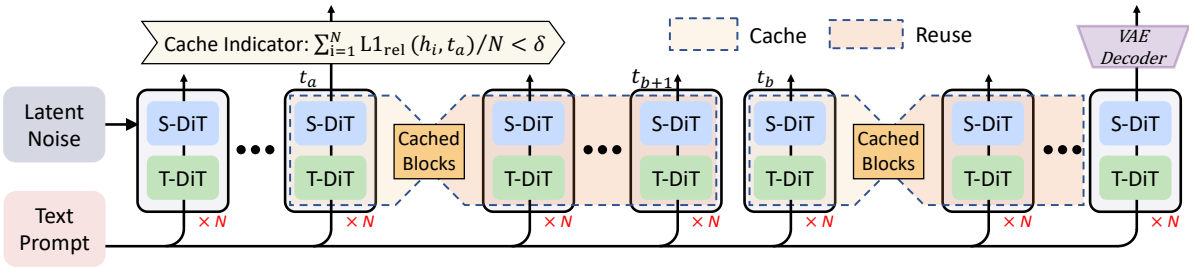

Figure 2: Overview of the BWCache. An indicator based on adjacent timestep differences in block features determines whether to reuse the cache. If conditions are met, subsequent timesteps reuse cached blocks; otherwise, blocks are recomputed and the cache updated.

blocks, specifically Spatial DiT (S-DiT) and Temporal DiT (T-DiT) blocks Ho et al. [2022]. However, these blocks must be executed in sequence, which considerably slows down inference. As a result, accelerating DiT inference has become one of the most pressing challenges faced by GenAI.

Traditional acceleration techniques for DMs primarily focus on architectural modifications such as distillation, pruning, and quantization Wang et al. [2024], Chu et al. [2024], Yang et al. [2024], Zhang et al. [2024a], Kang et al. [2024], Zhou et al. [2024]. Although these methods reduce model complexity, they also compromise generation quality. More importantly, they require substantial computational resources and extensive training data to fine-tune, which is impractical for large pre-trained DMs. A training-free alternative is to cache the intermediate features of DMs to accelerate inference Ma et al. [2023], Zhang et al. [2024b], Zhao et al. [2024a], Kahatapitiya et al. [2024], Liu et al. [2024]. By reusing these intermediate features across timesteps, these approaches eliminate redundant computations and significantly improve generation efficiency.

Despite the proven effectiveness of caching in accelerating DM inference, two critical challenges remain unresolved. First, DiT is a complex structure, considering caching at a coarse granularity (e.g., timesteps) Lv et al. [2024], Liu et al. [2024] may result in the loss of essential information, while considering caching at a fine granularity (e.g., attention) Kahatapitiya et al. [2024], Zhao et al. [2024a], Yuan et al. [2024], Zhang et al. [2025] often fails to deliver significant acceleration. Thus, the first challenge is to identify which features are appropriate for caching. Second, many existing methods assume high similarity between features across adjacent timesteps, sharing features between them to speed up inference Zhao et al. [2024a], Lv et al. [2024], Wimbauer et al. [2024], Selvaraju et al. [2024], Liu et al. [2025a]. In reality, however, feature similarity varies greatly depending on the generation task and specific inference process, and naive feature reuse can often degrade output details. Therefore, the second challenge is to determine when cached features should be reused or updated.

In this paper, we propose Block-Wise Caching (BWCache), a training-free method to accelerate DiT-based video generation. This method can be seamlessly integrated into most DiT-based models as a plug-and-play component during the inference phase. The core idea is to cache the features from all DiT blocks at certain diffusion timesteps and reuse them across several subsequent steps. Specifically, as shown in Figure 2, DiT-based video generation typically involves providing a text prompt and initializing latent noise, which is then refined through multiple iterative denoising steps, and finally reconstructed into video frames using a VAE decoder. To determine when to reuse cached features, we introduce a similarity indicator based on the differences between block features from adjacent timesteps. Periodic recomputation is applied to mitigate potential latent drift. This approach significantly reduces inference time and resource consumption while preserving output quality. We evaluate BWCache across several video diffusion models, including Open-Sora Zheng et al. [2024], Open-Sora-Plan Lin et al. [2024], and Latte Ma et al. [2025]. As shown in Figure 1, BWCache achieves superior performance at comparable computational costs to TeaCache Liu et al. [2024]. The main contributions are summarized as follows.

- We analyze the components of DiT-based models during the denoising process, revealing the dynamics within DiT blocks under different generation tasks and highlighting their similarities across specific diffusion timesteps.
- We propose BWCache, a training-free method compatible with DiT-based models that caches DiT block features and reuses them across multiple diffusion timesteps, thereby accelerating video generation inference.
- Experiments demonstrate that our method outperforms existing baselines in terms of inference speed and video generation quality, justified through both ablation studies and qualitative comparisons.

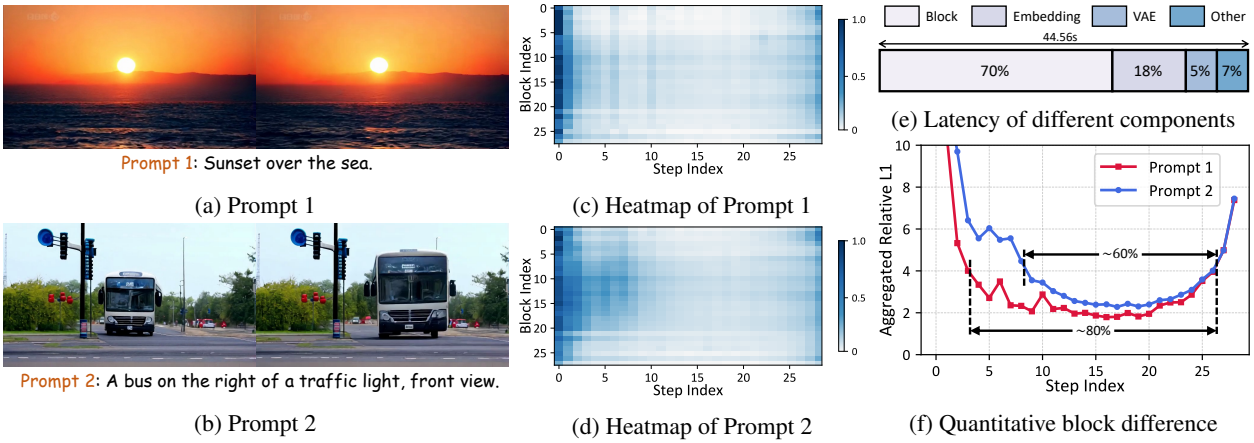

(a) Prompt 1 (b) Prompt 2 (c) Heatmap of Prompt 1 (d) Heatmap of Prompt 2 (e) Latency of different components (f) Quantitative block difference

Figure 3: Left: Two prompts and corresponding generated videos. Middle: Heatmap across 28 blocks and 30 denoising steps in Open-Sora. Right: Analysis of the block in the DiT-based model.

2 Related Work

2.1 Diffusion Model

Early video generation models, such as Variational Autoencoders (VAEs) Kingma et al. [2013] and Generative Adversarial Networks (GANs) Goodfellow et al. [2014], face several challenges, including blurry outputs, training instability, and limited text-video alignment. The emergence of DMs Ho et al. [2020], Dhariwal and Nichol [2021] addresses these limitations by achieving high-quality and diverse video generation through a gradual denoising process. Initially, these models employed U-Net architectures, which demonstrated impressive results in both image and video generation tasks Ramesh et al. [2022], Chen et al. [2024a], Wei et al. [2024]. More recently, advancements in DiT-based architectures Peebles and Xie [2023], Bao et al. [2023] have further improved scalability and generalization over traditional U-Net-based DMs. The success of the Sora model Brooks et al. [2024], which utilizes the DiT architecture for long-form video generation, has led to a growing body of research adopting DiT as the noise estimation network Hatamizadeh et al. [2024], Wang et al. [2025], Li et al. [2025].

2.2 Diffusion Model Acceleration

Despite the remarkable performance of DMs, their high inference costs limit their applicability in real-world applications. Existing acceleration techniques for DMs can generally be categorized into two groups. The first category relies on architectural changes, such as distillation simplifies networks Kang et al. [2024], Zhou et al. [2024], Salimans et al. [2024], pruning removes redundant parameters Yang et al. [2024], Zhang et al. [2024a], Castells et al. [2024], quantization reduces precision Wang et al. [2024], Chu et al. [2024], Huang et al. [2024a], and others. However, these approaches often require additional resources for fine-tuning or optimization. The second group consists of training-free methods that accelerate inference by caching intermediate features of diffusion models. DeepCache Ma et al. [2023] accelerates diffusion models by caching high-level features from sequential denoising timesteps. T-GATE Zhang et al. [2024b] enhances image generation efficiency by caching attention outputs. PAB Zhao et al. [2024a] leverages a U-shaped attention redundancy pattern to significantly accelerate the diffusion process. AdaCache Kahatapitiya et al. [2024] accelerates video generation by selectively caching computations based on video content. TeaCache Liu et al. [2024] utilizes timestep embeddings to dynamically determine which computations to cache to accelerate inference. Although these training-free methods enhance diffusion efficiency, they still face significant challenges in balancing generation quality with computational cost.

3 Methodology

3.1 Preliminaries

Denoising Diffusion Models. Consider the data $\mathbf{x}_0 \sim q(\mathbf{x})$ sampled from a real distribution. The forward diffusion process incrementally adds Gaussian noise over T steps, producing a sequence $\mathbf{x}_1, \ldots, \mathbf{x}_T$. As t increases, $\mathbf{x}_t$ progressively loses distinguishable features, asymptotically approaching an isotropic Gaussian distribution when

$T \to \infty$. With the Markov chain assumption, it is expressed as:

$$q(\mathbf{x}_t \,|\, \mathbf{x}_{t-1}) := \mathcal{N}(\mathbf{x}_t;\, \sqrt{1-\beta_t}\,\mathbf{x}_{t-1},\, \beta_t I), \tag{1}$$

where $q(\mathbf{x}_t|\mathbf{x}_{t-1})$ is the posterior probability. The step sizes are controlled by a noise schedule $\beta_1, \ldots, \beta_T$. The reverse process samples from $q(\mathbf{x}_{t-1}|\mathbf{x}_t)$ to reconstruct data from noise $\mathbf{x}_T \sim \mathcal{N}(\mathbf{0}, \mathbf{I})$. Similarly, the backward diffusion process can be written as:

$$p_\theta(\mathbf{x}_{t-1} \,|\, \mathbf{x}_t) := \mathcal{N}(\mathbf{x}_{t-1};\, \mu_\theta(\mathbf{x}_t, t),\, \Sigma_\theta(\mathbf{x}_t, t)), \tag{2}$$

where μ_θ and Σ_θ are learned parameters defining the mean and covariance, and $p_\theta(.)$ denotes the probability of observing $\mathbf{x}_{t-1}$ given $\mathbf{x}_t$.

DiT Block. The Spatial-Temporal DiT (ST-DiT) block Ho et al. [2022] follows the two-stage Transformer design to modulate the dynamics of diffusion features across both space and time. Each denoising step involves sequential processing through N consecutive DiT blocks. For the i-th DiT block ($i \in [1, N]$) in timestep t, given an input hidden state h_i, the block first performs Adaptive Layer Normalization (AdaLN) Xu et al. [2019] followed by multi-head self-attention:

$$h'_{t,i} = \mathrm{Attention}(\mathrm{AdaLN}(h_{t,i})) + h_{t,i}, \tag{3}$$

where the residual connection preserves input information. A subsequent AdaLN-modulated MLP enhances feature expression:

$$h''_{t,i} = \mathrm{MLP}(\mathrm{AdaLN}(h'_{t,i})) + h'_{t,i}. \tag{4}$$

The output hidden state $h''_{t,i}$ then becomes the input to the next DiT block (e.g., $h_{t,i+1} = h''_{t,i}$).

3.2 Analysis

Costs of Diffusion Models. The video generation process using DMs comprises multiple computational components, including the DiT blocks, timestep and text embeddings, VAE, and others. Figure 3(e) shows the time distribution for each part of the video generation process. As illustrated, the DiT blocks require considerably more computation time than the other components. Furthermore, this proportion increases further as the video length and resolution grow, posing a substantial challenge to the efficiency of video generation.

Block Feature Variation. To better understand the internal behavior of DiT blocks during video generation, we introduce the relative L1 distance Liu et al. [2024] to measure the feature variations of each block between adjacent timesteps. For the i-th block at the t-th step, the block-wise relative L1 distance is calculated as follows:

$$\mathrm{L1}_{\mathrm{rel}}(h_i, t) = \frac{\|h_{t,i} - h_{t+1,i}\|_1}{\|h_{t+1,i}\|_1}. \tag{5}$$

A smaller $\mathrm{L1}_{\mathrm{rel}}$ value indicates minimal feature variation within the block between adjacent timesteps, while a larger value shows significant changes. In Figures 3(a) and (b), we present two videos generated from different prompts. The video generated with Prompt 1 depicts a relatively static scene, whereas the video generated with Prompt 2 exhibits more dynamic content (e.g., a bus moving closer from a distance). To quantify the changes in block features during the generation process for both videos, we employ heatmaps, as shown in Figures 3(c) and (d). In these heatmaps, the color intensity reflects the relative degree of blokc feature variation at different timesteps, with darker regions indicating greater differences. From the figures, we observe two key insights: 1) the colors are darker in the initial and final timesteps, indicating that block features change across timesteps; 2) compared to Figure 3(d), the darker regions in Figure 3(c) occupy a smaller proportion, suggesting that different prompts exert varying influences on the features of the blocks.

Similarity and Diversity. To gain a more intuitive understanding of the changes in block feature at different timesteps, we aggregate the block-level feature differences within each timestep and define the aggregated relative L1 distance. The equation is as follows:

$$\mathrm{ARL1}(t) = \sum_{n=1}^{N} \mathrm{L1}_{\mathrm{rel}}(h_i, t), \tag{6}$$

where N is the total number of DiT blocks. $\mathrm{ARL1}(t)$ quantifies the feature change at a given diffusion step t by summing the relative L1 distances across all blocks.

Figure 3(f) illustrates the aggregated relative L1 distance for two prompts. Generally, the differences in block features between adjacent diffusion timesteps exhibit a U-shaped pattern. In the early timesteps, the L1 distance is high, indicating rapid changes in noise predictions. The middle timesteps gradually stabilize, showing considerable redundancy in block calculations. While in the final timesteps, the aggregated L1 distance increases, suggesting a transition from structured noise to high-fidelity video. Notably, for simpler or more static scenes, the feature variations among blocks stay minimal, explaining why Prompt 1 exhibits a longer duration of stable timesteps compared to Prompt 2.

3.3 BWCache

As illustrated in Figure 3, intermediate stages of video generation frequently exhibit redundant block computations. To minimize computational redundancy and accelerate inference, we propose Block-Wise Caching (BWCache). Instead of computing each DiT block at every timestep, we selectively reuse block features cached from the previous timestep. We employ the average of the accumulated relative L1 distance as a similarity indicator to determine when to reuse the cached blocks:

$$\sum_{n=1}^{N} \mathrm{L1}_{\mathrm{rel}}(h_i, t)/N < \delta, \tag{7}$$

where $\mathrm{L1}_{\mathrm{rel}}$ is defined in Eq.(5), and δ is the similarity threshold. Specifically, at each timestep, we calculate the relative L1 distance between each DiT block and its counterpart from the preceding timestep. After each timestep, we cache all block features and calculate the arithmetic mean of their relative L1 distances. If this mean is less than the indicator threshold δ, block computations can be skipped for subsequent timesteps starting from $t-1$, allowing the reuse of cached features; otherwise, the block will be recomputed. A smaller threshold δ reduces cache reuse, while a larger threshold speeds up video generation, but may adversely affect video quality. The appropriate threshold δ should be chosen to optimize inference speed without compromising visual quality.

Reusing DiT blocks in the final diffusion timesteps significantly degrades visual fidelity, as these timesteps represent the critical phase where the latent space transitions from structured noise to a high-quality video. Once BWCache is triggered at the k-th step, caching reuse is restricted to the first half of the remaining steps, while the second half is explicitly computed. Therefore, the last $k/2$ steps are always recomputed, ensuring thorough refinement during the most sensitive stage of generation.

Model	Method	Visual Quality				Efficiency		
		VBench↑	LPIPS↓	SSIM↑	PSNR↑	FLOPs (P)↓	Speedup↑	Latency(s)↓
Open-Sora	Original	80.33%	-	-	-	3.15	1×	44.56
	Δ-DiT	78.21%	0.5692	0.4811	11.91	3.09	1.03×	43.26
	T-GATE	77.61%	0.3495	0.6760	15.50	2.75	1.19×	37.45
	PAB	78.10%	0.2134	0.7798	22.02	2.55	1.38×	32.38
	TeaCache	79.16%	0.1496	0.8104	22.39	2.40	1.50×	29.64
	BWCache	**80.03%**	**0.0879**	**0.8854**	**27.05**	**2.32**	**1.61**×	**27.68**
Open-Sora-Plan	Original	80.88%	-	-	-	11.75	1×	99.65
	Δ-DiT	77.55%	0.5388	0.3736	13.85	11.74	1.01×	98.66
	T-GATE	80.15%	0.3066	0.6219	18.80	9.88	1.18×	84.45
	PAB	80.30%	0.2781	0.6627	19.49	8.69	1.36×	73.41
	TeaCache	80.32%	0.1965	0.7502	21.50	**3.13**	**4.41**×	**22.62**
	BWCache	**80.82%**	**0.1001**	**0.8435**	**25.87**	6.30	2.24×	44.49
Latte	Original	78.95%	-	-	-	3.36	1×	26.90
	Δ-DiT	52.00%	0.8513	0.1078	8.65	3.36	1.02×	26.37
	T-GATE	75.42%	0.2612	0.6927	19.55	2.99	1.13×	23.81
	PAB	76.32%	0.4625	0.5964	17.03	2.70	1.21×	22.16
	TeaCache	77.40%	0.1969	0.7606	22.19	1.86	1.86 ×	14.46
	BWCache	**78.28%**	**0.1399**	**0.8181**	**26.46**	**1.77**	**1.90**×	**14.16**

Table 1: Comparison of visual quality and efficiency on a single GPU. Video generation specifications: Open-Sora (51 frames, 480P), Open-Sora-Plan (65 frames, 512×512), Latte (16 frames, 512×512). LPIPS, SSIM, and PSNR are calculated against the original model results.

3.4 Periodic Cache Recomputation

Continuously reusing the same block may result in latent drift and gradually erase fine-grained details Liu et al. [2025b]. To prevent this cache stagnation, we adopt the progressive computation strategy from PAB Zhao et al. [2024a]: within the caching interval, each DiT block is periodically recomputed at a defined reuse interval R. Specifically, after computing the block at time step t, its features are cached and reused for the subsequent R steps (i.e., $[t-1, t-R]$),

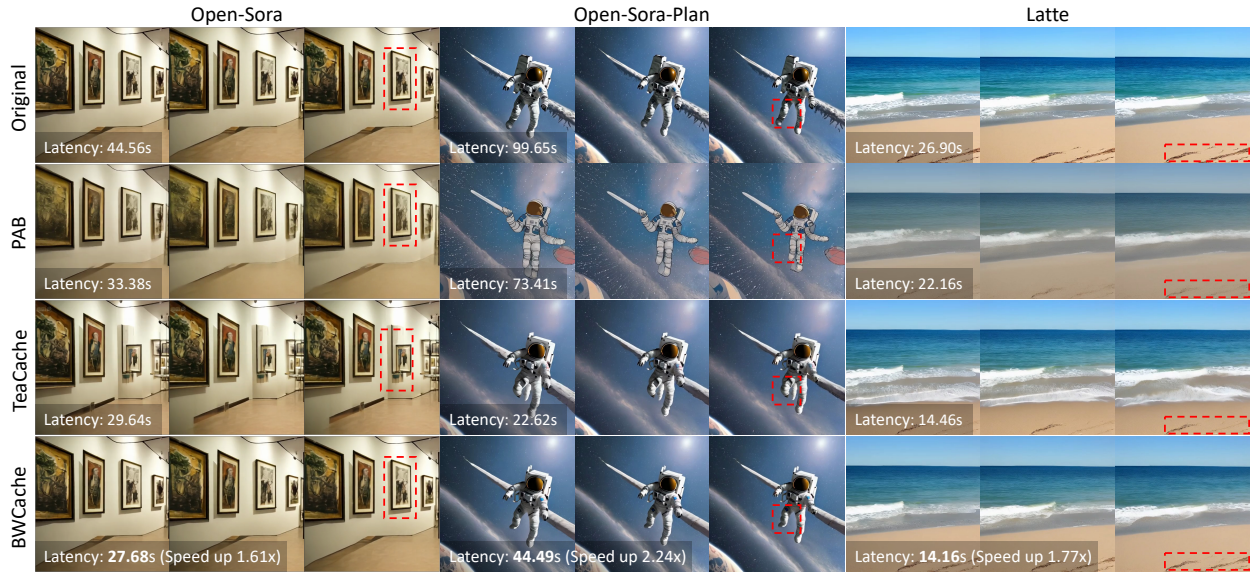

Figure 4: Comparison of visual quality and efficiency (denoted by latency) with the compared method. BWCache outperforms PAB and TeaCache in both visual quality and efficiency.

and the block is then updated at step $t - R - 1$. This process is formalized as:

$$\mathcal{O}_H = \{\ldots, \underbrace{h''_t}_{\text{cached}}, \underbrace{h''_t, \ldots, h''_t}_{\text{reuse } R \text{ steps}}, \underbrace{h''_{t-R-1}}_{\text{cached}}, \ldots\}, \tag{8}$$

where $\mathcal{O}_H$ denotes the output of the DiT block across all steps, and h''_t represents the DiT block output calculated at step t, which can be determined using Eq.(4).

4 Experimental Results

4.1 Experiment Setup

Base Models and Compared Methods. We apply the proposed acceleration techniques to various video generation diffusion models, including Open-Sora Zheng et al. [2024], Open-Sora-Plan Lin et al. [2024], and Latte Ma et al. [2025]. We compare our method with recent effective video generation techniques such as PAB Zhao et al. [2024a], T-GATE Zhang et al. [2024b], Δ-DiT Chen et al. [2024b], and TeaCache Liu et al. [2024] to highlight our advantages. The inference config of base models in Appendix 1.

Evaluation Metrics and Datasets. To evaluate the performance of video generation acceleration methods, we primarily focus on two aspects: visual quality and inference efficiency. We utilize VBench Huang et al. [2024b], LPIPS Zhang et al. [2018], PSNR, and SSIM Wang and Bovik [2002] for visual quality assessment. VBench is a comprehensive benchmarking suite for video generation models. LPIPS, PSNR, and SSIM measure the similarity between videos generated by the accelerated methods and the original models. Several evaluation metrics are detailed in Appendix 2. To assess inference efficiency, we use Floating Point Operations (FLOPs) and inference latency as metrics. In our main experiments, we generate over 1,000 videos for each model under each baseline using prompts sourced from Open-Sora gallery Lin et al. [2024], VBench benchmark Huang et al. [2024b], and T2V-CompBench Sun et al. [2024].

Implementation Details. All experiments are conducted on NVIDIA A800 80GB GPUs using PyTorch. FlashAttention Dao et al. [2022] is enabled by default across all experiments. Unless otherwise specified, ablation studies and qualitative analyses generate 51 frames, 480P videos in 30 steps. δ is set to 0.15 and reuse interval R is set to 10% of total timesteps by default.

4.2 Main Results

Quantitative Comparison. The experimental results in Table 1 demonstrate the effectiveness of BWCache across multiple DiT-based video generation models. Our proposed BWCache outperforms existing optimization methods

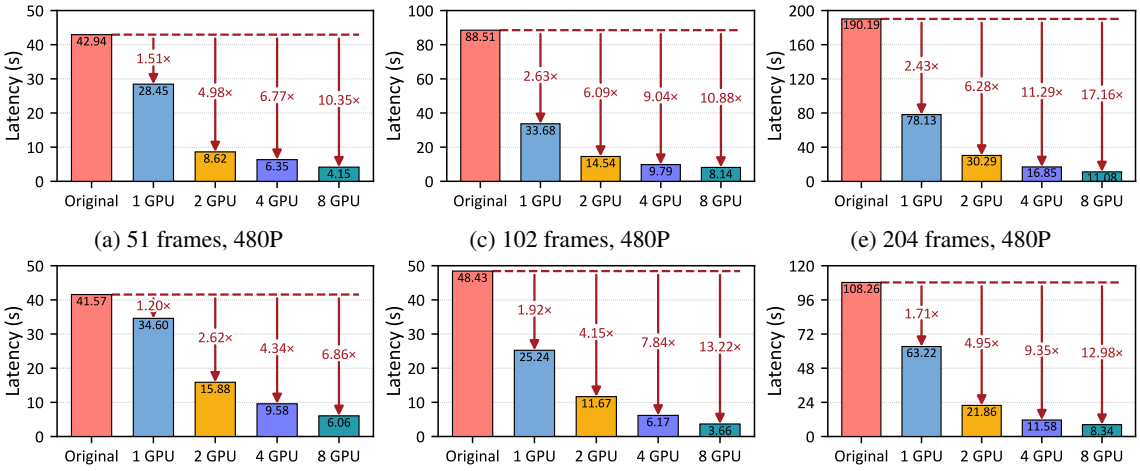

(a) 51 frames, 480P (c) 102 frames, 480P (e) 204 frames, 480P

(b) 204 frames, 240P (d) 102 frames, 360P (f) 51 frames, 720P

Figure 5: Inference efficiency of BWCache at different video lengths and resolutions.

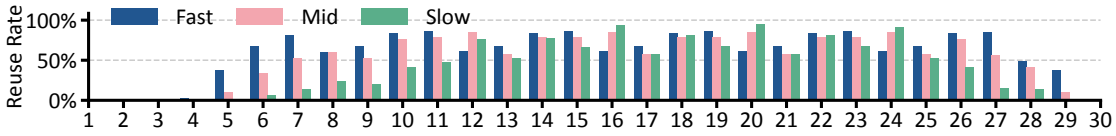

Figure 6: Visualization for the block reuse rate at each step.

in both visual quality and efficiency. For instance, on Open-Sora, BWCache achieves advanced visual metrics while reducing latency by 1.61× compared to the original model. Notably, BWCache surpasses the training-free TeaCache method and maintains competitive acceleration performance. The block-wise method of BWCache leverages DiT block redundancies more effectively without sacrificing visual details. The timestep-level caching of TeaCache is less adaptive to intra-timestep variations, leading to higher quality degradation. It is worth noting that TeaCache achieves faster acceleration than BWCache on the Open-Sora-Plan model. This is because there is significant variation in block features during the early inference stages of the Open-Sora-Plan model, and TeaCache focuses solely on input features while neglecting this variation. This aggressive acceleration strategy results in its generation quality lagging far behind that of BWCache. More experiments can be found in Appendix 3.

Visual Quality Comparison. As shown in Figure 4, we visualize the videos generated by our method compared to the original model, PAB, and TeaCache. The results demonstrate that BWCache outperforms other methods in visual quality with lower latency. More visual results are illustrated in Appendix 4.

4.3 Scaling Abilities

Scaling to Multiple GPUs. Table 2 summarizes the inference efficiency of various methods when scaled across multiple GPUs using Dynamic Sequence Parallelism (DSP) Zhao et al. [2024b]. The experiments, conducted using several models, reveal that BWCache consistently outperforms both the original model and PAB in terms of latency reduction across all tested scenarios. Specifically, BWCache achieves the lowest latencies, demonstrating significant speed-ups as the number of GPUs increases. These results validate BWCache as a universally effective acceleration method for DiT-based models under multi-GPU deployments.

Performance at Different Length and Resolution. Figure 5 demonstrates the inference efficiency of BWCache across various video lengths and resolutions using the Open-Sora model. The results show that latency increases significantly as the length and resolution of the video increased, but BWCache consistently performs better than the original model in all configurations. BWCache exhibits particularly notable acceleration advantages in processing high-resolution long videos. For example, with eight GPUs, BWCache attains a latency of just 11.08 seconds for the Open-Sora model with 204 frames at 480P, representing a remarkable 17.16× speed-up compared to the base model. This trend is also reflected in other configurations, where BWCache consistently provides substantial improvements in efficiency. Overall,

Method	1 × A800	2 × A800	4 × A800	8 × A800
Open-Sora (204 frames, 480P)				
original	190.2(1×)	71.3(2.7×)	37.7(5.1×)	24.1(7.9×)
PAB	150.7(1.2×)	55.3(3.3×)	29.8(6.1×)	19.8(9.1×)
Ours	**78.1(2.4×)**	**30.3(6.3×)**	**16.9(11.3×)**	**11.1(17.2×)**
Open-Sora-Plan (221 frames, 512×512)				
original	284.3(1×)	154.3(1.8×)	81.2(3.5×)	47.1(6.0×)
PAB	211.4(1.3×)	112.5(2.5×)	60.0(4.7×)	34.9(8.1×)
Ours	**109.1(2.6×)**	**60.0(4.7×)**	**32.8(8.7×)**	**21.4(13.3×)**
Latte (16 frames, 512×512)				
original	25.9(1×)	15.1(1.7×)	9.3(2.8×)	8.9(2.9×)
PAB	21.0(1.2×)	12.2(2.1×)	8.3(3.1×)	7.9(4.0×)
Ours	**14.4(1.8×)**	**7.3(3.6×)**	**4.5(5.8×)**	**4.0(6.5×)**

Table 2: Inference efficiency when scaling to multiple GPUs with DSP.

these results validate its capability to improve inference speeds across various video lengths and resolutions, making it an efficient solution for real-time video generation.

4.4 Ablation Studies

Quality-Efficiency Trade-Off. Figure 1 compares the quality-latency trade-off of BWCache, PAB, and TeaCache. The indicator threshold δ in Eq.(7) is 0.15, 0.20, and 0.25. The results clearly demonstrate that BWCache outperforms PAB and TeaCache in visual quality across all evaluated metrics, indicating a notable improvement in the fidelity of video generation. For each metric, BWCache not only achieves higher quality scores but also does so while maintaining lower latency, which reflects its efficient processing capabilities. Overall, BWCache achieves improved visual quality at lower latency than PAB and TeaCache.

Threshold	Reuse Rate	VBench↑	LPIPS↓	SSIM↑	PSNR↑
0.25(Fast)	59.00%	79.03%	0.1935	0.7829	21.39
0.20(Mid)	53.05%	79.42%	0.1486	0.8267	23.45
0.15(Slow)	41.38%	80.03%	0.0879	0.8854	27.05

Table 3: Impact of different reuse rates.

Reuse Rate. Table 3 illustrates how varying the reuse rates affects performance. It reveals that the “Fast" configuration achieves the highest reuse rate at 59.00%, resulting in the lowest latency of 19.16 seconds. The “Slow" configuration only had a reuse rate of 41.38%, but the visual quality is the highest among all configurations.

Visualized results in Figure 6 complement these findings by providing the reuse rates of blocks across each timestep for various thresholds. This figure illustrates the dynamic nature of block reuse at different timesteps, with evident fluctuations that suggest varying block reuse efficiency at different stages of video generation. In general, the block features in the middle stage of the generation change less, and a high reuse rate is obtained, which is consistent with our previous analysis.

Interval	Latency(s)↓	VBench↑	LPIPS↓	SSIM↑	PSNR↑
5%	34.70	80.28%	0.0451	0.9250	30.72
10%	27.68	80.03%	0.0879	0.8854	27.05
15%	27.33	79.84%	0.1065	0.8709	26.13
20%	25.97	79.48%	0.1415	0.8465	24.82
25%	25.76	79.31%	0.1567	0.8360	24.32

Table 4: Impact of different reuse intervals.

Reuse Interval. Table 4 outlines various reuse intervals, ranging from 5% to 25% of all timesteps, and details their corresponding latency and quality metrics. As the reuse interval increases, the latency decreases, indicating enhanced

generating efficiency. Conversely, while the latency improves with increased reuse interval, there is a slight degradation in quality metrics. For instance, VBench scores range from 80.28% at 5% to 79.31% at 25%, indicating a gradual decline in fidelity. This demonstrates a trade-off between latency and visual quality, where longer reuse intervals can effectively accelerate generation but may destroy the details in the output.

5 Conclusion

In this paper, we introduced BWCache, a novel caching method designed to accelerate video Diffusion Transformers. By analyzing feature dynamics in Spatial-Temporal DiT blocks, we established that block features across timesteps had significant computational redundancy. BWCache addressed this by employing dynamic block-wise caching and a similarity indicator, which selectively reused block features when their differences fell below a predefined threshold. Periodic recomputation was employed to mitigate potential latent drift. Extensive experiments demonstrated that BWCache achieved robust efficiency and visual quality across diverse generation models, sampling schedules, and video parameters. These results highlighted its potential for real-world applications. The current indicator threshold was preset, and future work will dynamically adjust the threshold according to different generation tasks.

References

Yang Song and Stefano Ermon. Generative modeling by estimating gradients of the data distribution. In *Advances in Neural Information Processing Systems (NeurIPS)*, volume 32, 2019.

Jonathan Ho, Ajay Jain, and Pieter Abbeel. Denoising diffusion probabilistic models. In *Advances in Neural Information Processing Systems (NeurIPS)*, volume 33, pages 6840–6851, 2020.

Prafulla Dhariwal and Alexander Nichol. Diffusion models beat gans on image synthesis. In *Advances in Neural Information Processing Systems (NeurIPS)*, volume 34, pages 8780–8794, 2021.

Robin Rombach, Andreas Blattmann, Dominik Lorenz, Patrick Esser, and Björn Ommer. High-resolution image synthesis with latent diffusion models. In *Proceedings of the IEEE/CVF Conference on Computer Vision and Pattern Recognition (CVPR)*, pages 10684–10695, 2022.

Olaf Ronneberger, Philipp Fischer, and Thomas Brox. U-net: Convolutional networks for biomedical image segmentation. In *International Conference on Medical image computing and computer-assisted intervention*, pages 234–241. Springer, 2015.

Aditya Ramesh, Prafulla Dhariwal, Alex Nichol, Casey Chu, and Mark Chen. Hierarchical text-conditional image generation with clip latents. *arXiv preprint arXiv:2204.06125*, 1(2):3, 2022.

Chitwan Saharia, William Chan, Saurabh Saxena, Lala Li, Jay Whang, Emily L Denton, Kamyar Ghasemipour, Raphael Gontijo Lopes, Burcu Karagol Ayan, Tim Salimans, et al. Photorealistic text-to-image diffusion models with deep language understanding. In *Advances in Neural Information Processing Systems (NeurIPS)*, volume 35, pages 36479–36494, 2022.

Andreas Blattmann, Tim Dockhorn, Sumith Kulal, Daniel Mendelevitch, Maciej Kilian, Dominik Lorenz, Yam Levi, Zion English, Vikram Voleti, Adam Letts, et al. Stable video diffusion: Scaling latent video diffusion models to large datasets. *arXiv preprint arXiv:2311.15127*, 2023.

Tim Brooks, Bill Peebles, Connor Holmes, Will DePue, Yufei Guo, Li Jing, David Schnurr, Joe Taylor, Troy Luhman, Eric Luhman, Clarence Ng, Ricky Wang, and Aditya Ramesh. Video generation models as world simulators, 2024.

William Peebles and Saining Xie. Scalable diffusion models with transformers. In *Proceedings of the IEEE/CVF International Conference on Computer Vision (ICCV)*, pages 4195–4205, 2023.

Fan Bao, Shen Nie, Kaiwen Xue, Yue Cao, Chongxuan Li, Hang Su, and Jun Zhu. All are worth words: A vit backbone for diffusion models. In *Proceedings of the IEEE/CVF Conference on Computer Vision and Pattern Recognition (CVPR)*, pages 22669–22679, 2023.

Jonathan Ho, Tim Salimans, Alexey Gritsenko, William Chan, Mohammad Norouzi, and David J Fleet. Video diffusion models. In *Advances in Neural Information Processing Systems (NeurIPS)*, volume 35, pages 8633–8646, 2022.

Changyuan Wang, Ziwei Wang, Xiuwei Xu, Yansong Tang, Jie Zhou, and Jiwen Lu. Towards accurate post-training quantization for diffusion models. In *Proceedings of the IEEE/CVF Conference on Computer Vision and Pattern Recognition (CVPR)*, pages 16026–16035, 2024.

Huanpeng Chu, Wei Wu, Chengjie Zang, and Kun Yuan. Qncd: Quantization noise correction for diffusion models. In *Proceedings of the ACM International Conference on Multimedia (ACM MM)*, pages 10995–11003, 2024.

Tianyun Yang, Juan Cao, and Chang Xu. Pruning for robust concept erasing in diffusion models. *arXiv preprint arXiv:2405.16534*, 2024.

Dingkun Zhang, Sijia Li, Chen Chen, Qingsong Xie, and Haonan Lu. Laptop-diff: Layer pruning and normalized distillation for compressing diffusion models. *arXiv preprint arXiv:2404.11098*, 2024a.

Minguk Kang, Richard Zhang, Connelly Barnes, Sylvain Paris, Suha Kwak, Jaesik Park, Eli Shechtman, Jun-Yan Zhu, and Taesung Park. Distilling diffusion models into conditional gans. In *Proceedings of the European Conference on Computer Vision (ECCV)*, pages 428–447, 2024.

Zhenyu Zhou, Defang Chen, Can Wang, Chun Chen, and Siwei Lyu. Simple and fast distillation of diffusion models. In *Advances in Neural Information Processing Systems (NeurIPS)*, volume 37, pages 40831–40860, 2024.

Xinyin Ma, Gongfan Fang, and Xinchao Wang. Deepcache: Accelerating diffusion models for free. *arXiv preprint arXiv:2312.00858*, 2023.

Wentian Zhang, Haozhe Liu, Jinheng Xie, Francesco Faccio, Mike Zheng Shou, and Jürgen Schmidhuber. Cross-attention makes inference cumbersome in text-to-image diffusion models. *arXiv preprint arXiv:2404.02747v1*, 2024b.

Xuanlei Zhao, Xiaolong Jin, Kai Wang, and Yang You. Real-time video generation with pyramid attention broadcast. *arXiv preprint arXiv:2408.12588*, 2024a.

Kumara Kahatapitiya, Haozhe Liu, Sen He, Ding Liu, Menglin Jia, Chenyang Zhang, Michael S. Ryoo, and Tian Xie. Adaptive caching for faster video generation with diffusion transformers. *arXiv preprint arXiv:2411.02397*, 2024.

Feng Liu, Shiwei Zhang, Xiaofeng Wang, Yujie Wei, Haonan Qiu, Yuzhong Zhao, Yingya Zhang, Qixiang Ye, and Fang Wan. Timestep embedding tells: It's time to cache for video diffusion model. *arXiv preprint arXiv:2411.19108*, 2024.

Zhengyao Lv, Chenyang Si, Junhao Song, Zhenyu Yang, Yu Qiao, Ziwei Liu, and Kwan-Yee K Wong. Fastercache: Training-free video diffusion model acceleration with high quality. *arXiv preprint arXiv:2410.19355*, 2024.

Zhihang Yuan, Hanling Zhang, Lu Pu, Xuefei Ning, Linfeng Zhang, Tianchen Zhao, Shengen Yan, Guohao Dai, and Yu Wang. Ditfastattn: Attention compression for diffusion transformer models. In *Advances in Neural Information Processing Systems (NeurIPS)*, volume 37, pages 1196–1219, 2024.

Hanling Zhang, Rundong Su, Zhihang Yuan, Pengtao Chen, Mingzhu Shen Yibo Fan, Shengen Yan, Guohao Dai, and Yu Wang. Ditfastattnv2: Head-wise attention compression for multi-modality diffusion transformers. *arXiv preprint arXiv:2503.22796*, 2025.

Felix Wimbauer, Bichen Wu, Edgar Schoenfeld, Xiaoliang Dai, Ji Hou, Zijian He, Artsiom Sanakoyeu, Peizhao Zhang, Sam Tsai, Jonas Kohler, et al. Cache me if you can: Accelerating diffusion models through block caching. In *Proceedings of the IEEE/CVF Conference on Computer Vision and Pattern Recognition (CVPR)*, pages 6211–6220, 2024.

Pratheba Selvaraju, Tianyu Ding, Tianyi Chen, Ilya Zharkov, and Luming Liang. Fora: Fast-forward caching in diffusion transformer acceleration. *arXiv preprint arXiv:2407.01425*, 2024.

Joseph Liu, Joshua Geddes, Ziyu Guo, Haomiao Jiang, and Mahesh Kumar Nandwana. Smoothcache: A universal inference acceleration technique for diffusion transformers. In *Proceedings of the IEEE/CVF Conference on Computer Vision and Pattern Recognition (CVPR)*, pages 3229–3238, 2025a.

Zangwei Zheng, Xiangyu Peng, Tianji Yang, Chenhui Shen, Shenggui Li, Hongxin Liu, Yukun Zhou, Tianyi Li, and Yang You. Open-sora: Democratizing efficient video production for all. *arXiv preprint arXiv:2412.20404*, 2024.

Bin Lin, Yunyang Ge, Xinhua Cheng, Zongjian Li, Bin Zhu, Shaodong Wang, Xianyi He, Yang Ye, Shenghai Yuan, Liuhan Chen, et al. Open-sora plan: Open-source large video generation model. *arXiv preprint arXiv:2412.00131*, 2024.

Xin Ma, Yaohui Wang, Xinyuan Chen, Gengyun Jia, Ziwei Liu, Yuan-Fang Li, Cunjian Chen, and Yu Qiao. Latte: Latent diffusion transformer for video generation. *Transactions on Machine Learning Research*, 2025.

Diederik P Kingma, Max Welling, et al. *Auto-encoding variational bayes*. Banff, Canada, 2013.

Ian Goodfellow, Jean Pouget-Abadie, Mehdi Mirza, Bing Xu, David Warde-Farley, Sherjil Ozair, Aaron Courville, and Yoshua Bengio. Generative adversarial nets. In *Advances in Neural Information Processing Systems (NeurIPS)*, volume 27, 2014.

Haoxin Chen, Yong Zhang, Xiaodong Cun, Menghan Xia, Xintao Wang, Chao Weng, and Ying Shan. Videocrafter2: Overcoming data limitations for high-quality video diffusion models. In *Proceedings of the IEEE/CVF Conference on Computer Vision and Pattern Recognition (CVPR)*, pages 7310–7320, 2024a.

Yujie Wei, Shiwei Zhang, Zhiwu Qing, Hangjie Yuan, Zhiheng Liu, Yu Liu, Yingya Zhang, Jingren Zhou, and Hongming Shan. Dreamvideo: Composing your dream videos with customized subject and motion. In *Proceedings of the IEEE/CVF Conference on Computer Vision and Pattern Recognition (CVPR)*, pages 6537–6549, 2024.

Ali Hatamizadeh, Jiaming Song, Guilin Liu, Jan Kautz, and Arash Vahdat. Diffit: Diffusion vision transformers for image generation. In *Proceedings of the European Conference on Computer Vision (ECCV)*, pages 37–55. Springer, 2024.

Yaohui Wang, Xinyuan Chen, Xin Ma, Shangchen Zhou, Ziqi Huang, Yi Wang, Ceyuan Yang, Yinan He, Jiashuo Yu, Peiqing Yang, et al. Lavie: High-quality video generation with cascaded latent diffusion models. *International Journal of Computer Vision*, 133:3059–3078, 2025.

Zijie Li, Henry Li, Yichun Shi, Amir Barati Farimani, Yuval Kluger, Linjie Yang, and Peng Wang. Dual diffusion for unified image generation and understanding. In *Proceedings of the IEEE/CVF Conference on Computer Vision and Pattern Recognition (CVPR)*, pages 2779–2790, 2025.

Tim Salimans, Thomas Mensink, Jonathan Heek, and Emiel Hoogeboom. Multistep distillation of diffusion models via moment matching. In *Advances in Neural Information Processing Systems (NeurIPS)*, volume 37, pages 36046–36070, 2024.

Thibault Castells, Hyoung-Kyu Song, Bo-Kyeong Kim, and Shinkook Choi. Ld-pruner: Efficient pruning of latent diffusion models using task-agnostic insights. In *Proceedings of the IEEE/CVF Conference on Computer Vision and Pattern Recognition (CVPR)*, pages 821–830, 2024.

Yushi Huang, Ruihao Gong, Jing Liu, Tianlong Chen, and Xianglong Liu. Tfmq-dm: Temporal feature maintenance quantization for diffusion models. In *Proceedings of the IEEE/CVF Conference on Computer Vision and Pattern Recognition (CVPR)*, pages 7362–7371, 2024a.

Jingjing Xu, Xu Sun, Zhiyuan Zhang, Guangxiang Zhao, and Junyang Lin. Understanding and improving layer normalization. In *Advances in Neural Information Processing Systems (NeurIPS)*, volume 32, 2019.

Dong Liu, Jiayi Zhang, Yifan Li, Yanxuan Yu, Ben Lengerich, and Ying Nian Wu. Fastcache: Fast caching for diffusion transformer through learnable linear approximation. *arXiv preprint arXiv:2505.20353*, 2025b.

Pengtao Chen, Mingzhu Shen, Peng Ye, Jianjian Cao, Chongjun Tu, Christos-Savvas Bouganis, Yiren Zhao, and Tao Chen. $delta$-dit: A training-free acceleration method tailored for diffusion transformers. *arXiv preprint arXiv:2406.01125*, 2024b.

Ziqi Huang, Yinan He, Jiashuo Yu, Fan Zhang, Chenyang Si, Yuming Jiang, Yuanhan Zhang, Tianxing Wu, Qingyang Jin, Nattapol Chanpaisit, Yaohui Wang, Xinyuan Chen, Limin Wang, Dahua Lin, Yu Qiao, and Ziwei Liu. VBench: Comprehensive benchmark suite for video generative models. In *Proceedings of the IEEE/CVF Conference on Computer Vision and Pattern Recognition (CVPR)*, 2024b.

Richard Zhang, Phillip Isola, Alexei A Efros, Eli Shechtman, and Oliver Wang. The unreasonable effectiveness of deep features as a perceptual metric. In *Proceedings of the IEEE/CVF Conference on Computer Vision and Pattern Recognition (CVPR)*, 2018.

Zhou Wang and Alan C Bovik. A universal image quality index. *IEEE signal processing letters*, 9(3):81–84, 2002.

Kaiyue Sun, Kaiyi Huang, Xian Liu, Yue Wu, Zihan Xu, Zhenguo Li, and Xihui Liu. T2v-compbench: A comprehensive benchmark for compositional text-to-video generation. *arXiv preprint arXiv:2407.14505*, 2024.

Tri Dao, Daniel Y. Fu, Stefano Ermon, Atri Rudra, and Christopher Ré. FlashAttention: Fast and memory-efficient exact attention with IO-awareness. In *Advances in Neural Information Processing Systems (NeurIPS)*, 2022.

Xuanlei Zhao, Shenggan Cheng, Chang Chen, Zangwei Zheng, Ziming Liu, Zheming Yang, and Yang You. Dsp: Dynamic sequence parallelism for multi-dimensional transformers. *arXiv preprint arXiv:2403.10266*, 2024b.

A Experimental Settings

Base Model. This paper focuses on DiT-based video generation, evaluating three state-of-the-art open-source models: Open-Sora Zheng et al. [2024], Open-Sora-Plan Lin et al. [2024], and Latte Ma et al. [2025]. Open-Sora employs Spatial-Temporal DiT Ho et al. [2022], allowing for the creation of videos up to 16 seconds long at 720p resolution. Open-Sora Plan focuses on generating high-resolution videos with extended durations based on diverse user inputs, featuring components like a Wavelet-Flow Variational Autoencoder and specialized denoisers. Latte effectively extracts spatio-temporal tokens from videos and utilizes DiT blocks to model the token distribution in a latent space. The inference configs of three models are shown in Table 5, which strictly follow the official settings.

Model	Scheduler	Steps	Text Encoder
Open-Sora	RFLOW	30	T5
Open-Sora-Plan	PNDM	150	T5
Latte	DDIM	50	T5

Table 5: The inference config of base models.

Figure 7: Accelerate video generation by reducing inference steps and using caching respectively.

B Metrics

Peak Signal-to-Noise Ratio (PSNR). PSNR is a common metric used to measure the quality of reconstruction in lossy compression and signal processing. It compares the maximum possible power of a signal to the power of corrupting noise. Higher PSNR values indicate better quality. The PSNR is calculated as follows:

$$\text{PSNR} = 10 \cdot \log_{10}\left(\frac{R^2}{\text{MSE}}\right) \tag{9}$$

where R is the maximum possible pixel value of the image and MSE denotes the Mean Squared Error between the reference image and the reconstructed image.

Learned Perceptual Image Patch Similarity (LPIPS). LPIPS Zhang et al. [2018] is a modern perceptual similarity metric that is based on deep learning. It quantifies the similarity between two images by comparing their features at different layers of a neural network. This metric is believed to better correlate with human visual perception than traditional metrics by capturing perceptually important features. The LPIPS score between two images I and K is typically computed as:

$$\text{LPIPS}(I, K) = \frac{1}{L}\sum_{l=1}^{L} \|\phi_l(I) - \phi_l(K)\|^2 \tag{10}$$

where L is the number of layers in the pretrained neural network, and ϕ_l denotes the feature extraction at layer l. For video evaluation, LPIPS is calculated for each frame of the video and averaged across all frames to produce a final score.

Structural Similarity Index Measure (SSIM). SSIM Wang and Bovik [2002] is a perceptual metric that assesses the visual impact of three characteristics: luminance, contrast, and structure. Instead of measuring pixel-wise differences, SSIM compares the structural information in the images, making it a more relevant measure of perceived quality. The SSIM index is calculated as follows:

$$SSIM(I, K) = \frac{(2\mu_I\mu_K + C_1)(2\sigma_{IK} + C_2)}{(\mu_I^2 + \mu_K^2 + C_1)(\sigma_I^2 + \sigma_K^2 + C_2)} \tag{11}$$

where μ_I and μ_K are the average luminance of I and K, σ_I^2 and σ_K^2 are the variances of I and K, σ_{IK} is the covariance between I and K, C_1 and C_2 are constants used to stabilize the division with weak denominator. For video evaluation, SSIM is calculated for each frame and then averaged over all frames to provide an overall similarity measure.

Models	Subject Consistency	Background Consistency	Temporal Flickering	Motion Smoothness	Dynamic Degree	Aesthetic Quality	Imaging Quality	Object Class
Original	95.08%	96.86%	99.41%	98.80%	42.00%	59.53%	62.60%	95.87%
PAB	95.15%	96.70%	99.38%	99.09%	28.00%	56.32%	59.63%	96.37%
TeaCache	95.33%	96.83%	99.44%	98.94%	36.00%	58.50%	59.79%	96.00%
BWCache	95.91%	96.76%	99.43%	98.97%	38.00%	59.26%	61.29%	98.25%
Empirical Min	14.62%	26.15%	62.93%	70.60%	0.00%	0.00%	0.00%	0.00%
Empirical Max	100.00%	100.00%	100.00%	99.75%	100.00%	100.00%	100.00%	100.00%

Models	Multiple Objects	Human Action	Color	Spatial Relationship	Scene	Appearance Style	Temporal Style	Overall Consistency
Original	36.00%	84.00%	81.25%	85.75%	59.62%	25.40%	23.03%	27.90%
PAB	38.50%	68.00%	85.64%	77.22%	57.37%	25.06%	22.20%	26.70%
TeaCache	31.50%	82.00%	81.61%	85.75%	56.13%	24.93%	22.73%	27.24%
BWCache	36.25%	84.00%	82.58%	86.52%	59.25%	25.27%	22.74%	27.91%
Empirical Min	0.00%	0.00%	0.00%	0.00%	0.00%	0.00%	0.00%	0.00%
Empirical Max	100.00%	100.00%	100.00%	100.00%	82.22%	28.55%	36.40%	36.40%

Table 6: VBench evaluation results per dimension.

Last Step	Latency(s)↓	Vbench↑	LPIPS↓	SSIM↑	PSNR↑
$1/3k$	29.10	79.95%	0.0922	0.8823	26.95
$1/2k$	27.68	80.03%	0.0879	0.8854	27.05
$2/3k$	25.98	80.09%	0.0853	0.8874	27.16
5	31.47	80.13%	0.0877	0.8866	27.10
8	28.62	80.00%	0.0862	0.8896	27.01

Table 7: Impact of different last steps.

C Additional Experimental Results

C.1 Full Vbench Results.

VBench Huang et al. [2024b] is a comprehensive benchmark suite designed for evaluating video generative models. It provides a standardized framework that includes diverse evaluation metrics, datasets, and protocols to facilitate in-depth comparisons of model performance across various tasks. This systematic approach ensures reliable assessments of generated videos in terms of quality, efficiency, and robustness. Table 6 compares the performance of four video generation methods across each of the 16 VBench dimensions. A higher score indicates relatively better performance for a particular dimension. We also provide two specially built baselines, i.e., Empirical Min and Max (the approximated achievable min and max scores for each dimension), as references.

C.2 Last Step

In the final stage of the DiT model for video generation, that is, during the last stage of denoising, the reuse of cached block features can introduce unnecessary biases and lead to a degradation in the generated video. Therefore, assuming that cache reuse is triggered at the k-th step during the denoising process, we default that the last $1/2k$ steps do not involve cache and reuse operations. Meanwhile, we have statistically analyzed the results for the last $1/3k$ and $2/3k$ steps, as well as fixed 5 and 8 steps, as shown in Table 7. It can be seen that the choice of the last steps has a significant impact on latency and video generation quality. Specifically, as the number of last steps increases, latency tends to decrease, while metrics exhibit fluctuations to some extent. In general, our default setting $1/2k$ balances the generation quality and latency.

C.3 Reducing Inference Steps

When generating videos using the DiT model, the impact of the inference steps must be considered. Although increasing the inference steps can enhance video quality, it clearly requires higher GPU usage and increases the generation latency. In this paper, the default setting for the inference steps in Open-Sora is 30. To accelerate video generation, the number of inference steps can be reduced. We compare the performance of the original model with reduced inference steps and BWCache in terms of visual quality and latency. The results show that, while producing similar latencies, BWCache maintains excellent visual quality, as shown in Figure 7. Specific data on visual quality and efficiency is

Method	Latency(s)↓	LPIPS↓	SSIM↑	PSNR↑
original, 19 steps	29.20	0.3139	0.6922	16.39
BWCache, 30 steps	27.68	0.0879	0.8856	27.08

Table 8: Caching mechanism v.s. inference steps.

Model	Method	Metrics	Mean	Standard Deviation	P-Value	Confidence Interval
Open-Sora	PAB	LPIPS	0.2134	0.1026	9.90e-111	[0.2048, 0.2220]
		SSIM	0.7798	0.1084	8.99e-73	[0.7707, 0.7888]
		PSNR	22.0191	2.8325	2.8e-135	[21.7819, 22.2564]
	TeaCache	LPIPS	0.1496	0.0780	1.07e-46	[0.1430, 0.1561]
		SSIM	0.8104	0.1034	1.09e-42	[0.8017, 0.8190]
		PSNR	22.3929	4.3654	2.8e-80	[22.0273, 22.7586]
	BWCache	LPIPS	0.0879	0.0561	-	[0.0832, 0.0926]
		SSIM	0.8854	0.0665	-	[0.8798, 0.8909]
		PSNR	27.0510	2.9898	-	[26.8006, 27.3014]
Open-Sora-Plan	PAB	LPIPS	0.2781	0.1177	7.69e-51	[0.2602, 0.2961]
		SSIM	0.6627	0.1449	7.16e-37	[0.6407, 0.6848]
		PSNR	19.4968	3.6949	6.76e-42	[18.9340, 20.0596]
	TeaCache	LPIPS	0.1965	0.0928	6.64e-27	[0.1824, 0.2106]
		SSIM	0.7502	0.1090	4.95e-18	[0.7336, 0.7668]
		PSNR	21.5010	3.5785	6.25e-24	[20.9559, 22.0461]
	BWCache	LPIPS	0.1001	0.0520	-	[0.0922, 0.1080]
		SSIM	0.8435	0.0743	-	[0.8322, 0.8548]
		PSNR	25.8734	3.7611	-	[25.3006, 26.4463]
Latte	PAB	LPIPS	0.4625	0.1481	3.84e-218	[0.4501, 0.4750]
		SSIM	0.5964	0.1631	3.88e-106	[0.5827, 0.6100]
		PSNR	17.0299	2.2196	2.67e-189	[16.8440, 17.2158]
	TeaCache	LPIPS	0.1969	0.1058	5.32e-17	[0.1880, 0.2058]
		SSIM	0.7606	0.1329	2.39e-12	[0.7495, 0.7718]
		PSNR	22.1947	4.3783	1.02e-40	[21.8280, 22.5614]
	BWCache	LPIPS	0.1399	0.1160	-	[0.1301, 0.1496]
		SSIM	0.8181	0.1357	-	[0.8067, 0.8294]
		PSNR	26.4620	5.6981	-	[25.9847, 26.9392]

Table 9: Statistical comparison of the BWCache with compared methods.

detailed in Table 8. Overall, when the number of inference steps is reduced, sampling trajectories deviate from the theoretical optimal path, which amplifies accumulated errors in the noise estimation network. This results in issues such as blurred video details and reduced color saturation. BWCache maintains a high-fidelity video by caching and reusing intermediate stages of inference and their similar DiT block features, thus significantly reducing latency while accurately reconstructing the original inference process.

C.4 Statistical Analysis

TABLE 9 shows the statistical results of the paired t-test that determine the significance level of the BWCache compared with other methods regarding LPIPS, SSIM, and PSNR. Specifically, the table provides the mean and standard deviation of PAB Zhao et al. [2024a] and TeaCache Liu et al. [2024], alongside the p-value and corresponding confidence interval. Our null hypothesis is: “There is no significant difference in the performance between the BWCache and other methods". The table shows a meaningful difference between the BWCache and other methods, while the p-value is lower than 0.05 in all cases. There is statistically significant evidence at the 5% significance level to suggest that the BWCache performs better than PAB and TeaCache. Thus, the null hypothesis is rejected, which proves that differences are significant.

D More visual results

The additional visual comparison results for Open-Sora, Open-Sora-Plan, and Latte are presented in Fig. 8, Fig. 9, and Fig. 10. All prompts sourced from the Open-Sora gallery Lin et al. [2024], VBench benchmark Huang et al. [2024b], and T2V-CompBench Sun et al. [2024], which collectively offer diverse and representative scenarios for comprehensive

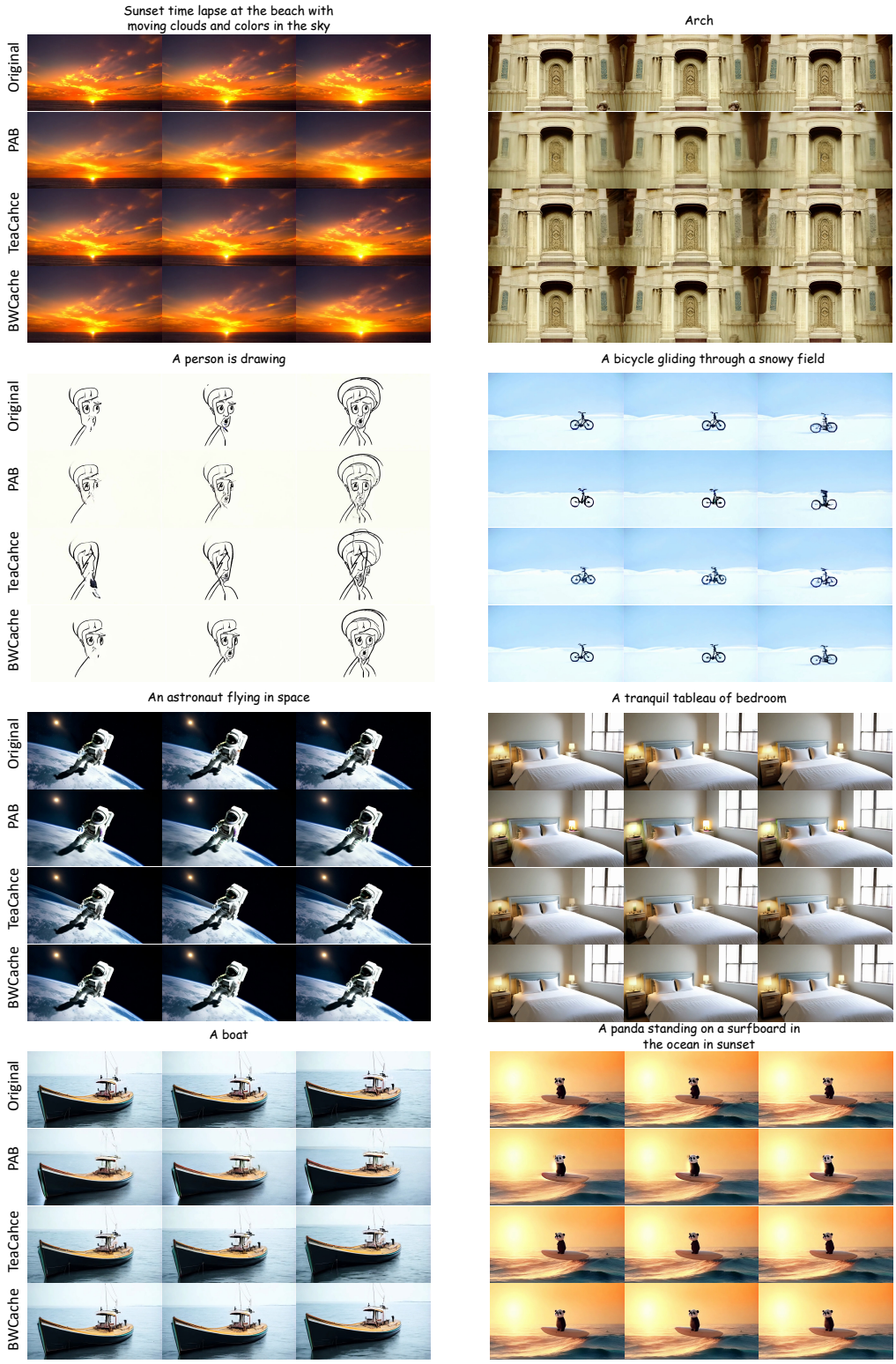

Figure 8: More visual results on Open-Sora (51 frames, 480P).

evaluation. Our method demonstrates consistent fidelity across diverse models, styles, and content types in video generation while maintaining computational efficiency.

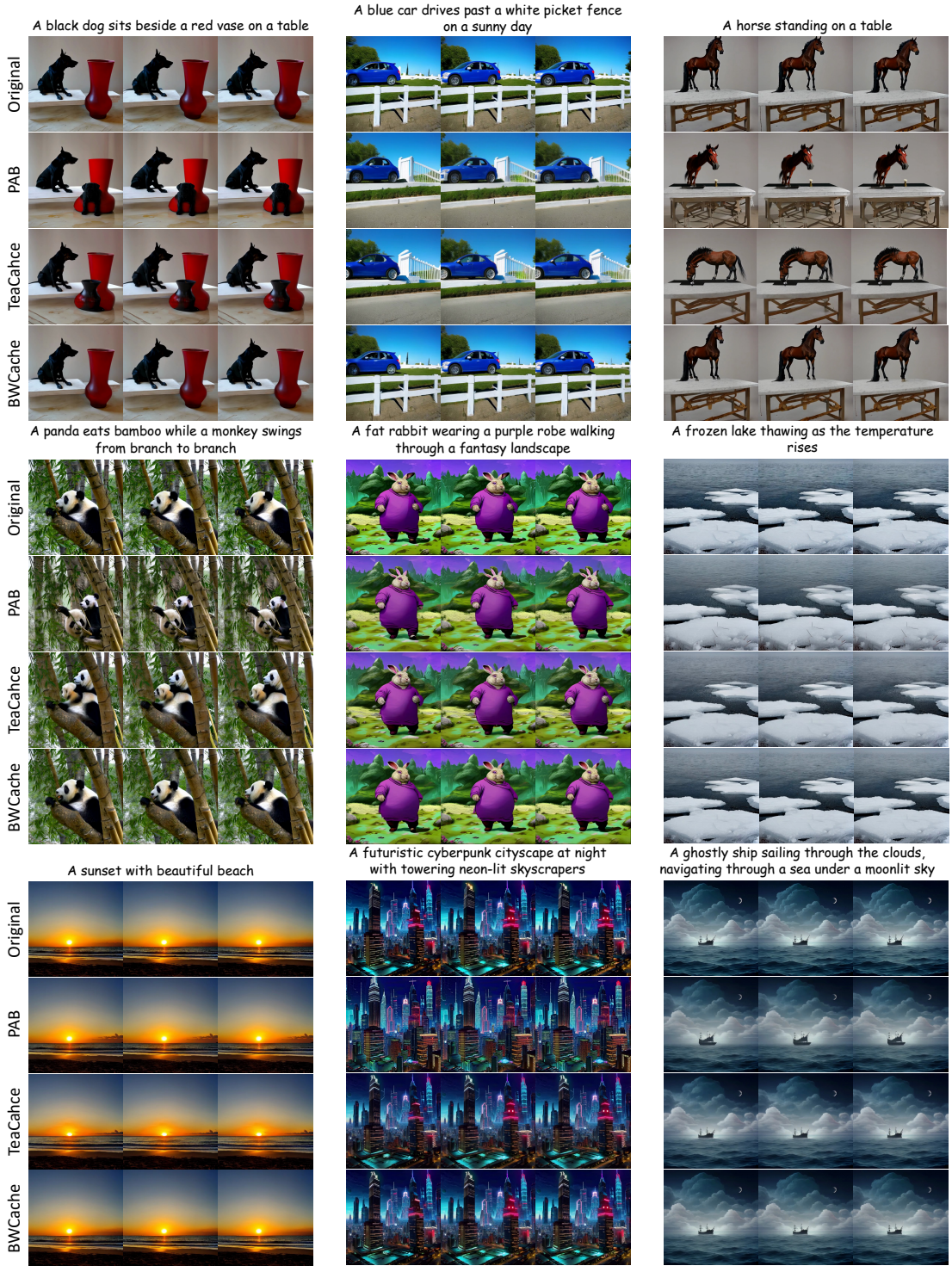

Figure 9: More visual results on Open-Sora-Plan (65 frames, 512×512).

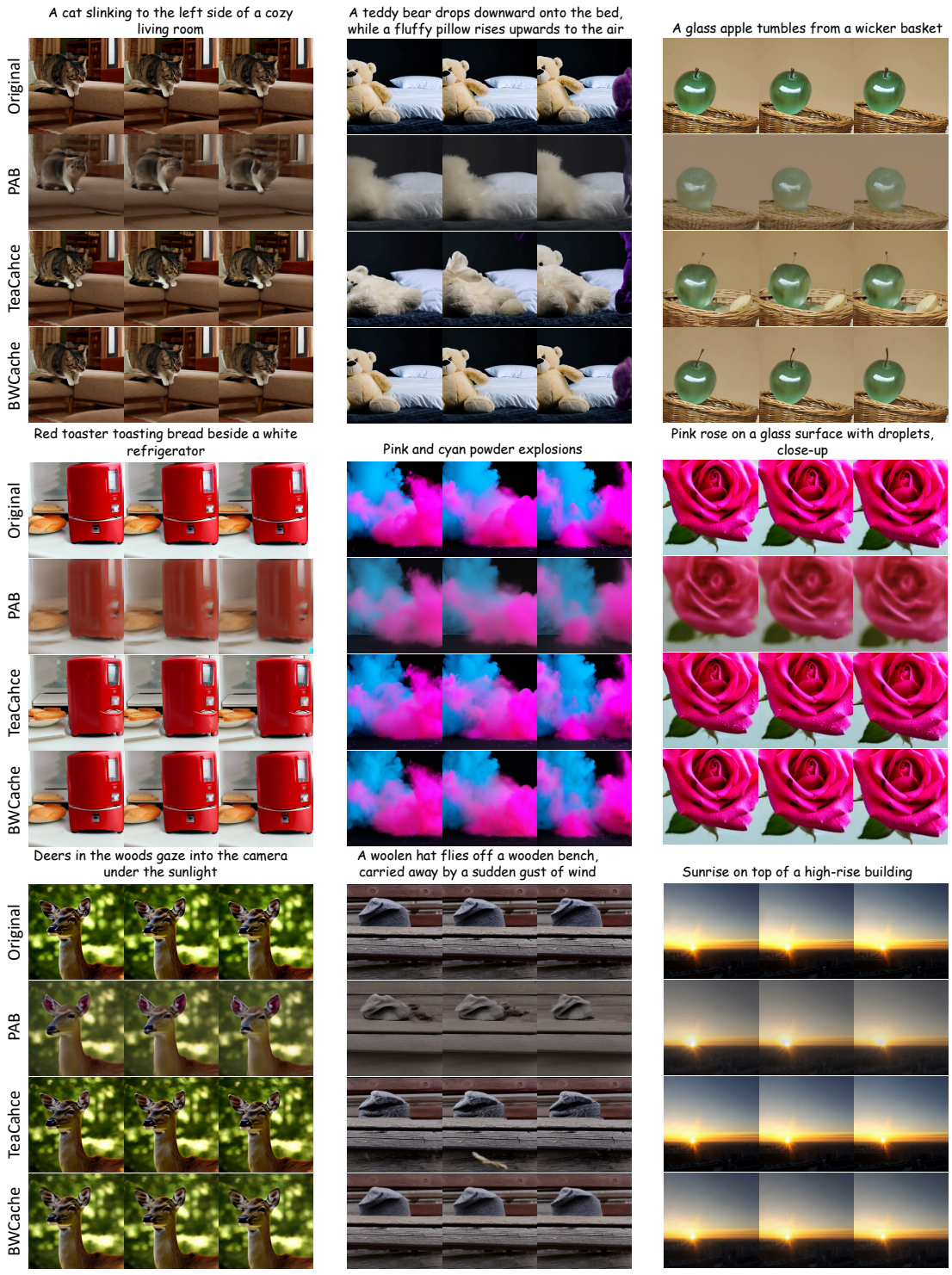

Figure 10: More visual results on Latte (16 frames, 512×512).